ChemComm

Chemical Communications

Accepted Manuscript

Published on 17 July 2026

This is an Accepted Manuscript, which has been through the Royal Society of Chemistry peer review process and has been accepted for publication.

Accepted Manuscripts are published online shortly after acceptance, before technical editing, formatting and proof reading. Using this free service, authors can make their results available to the community, in citable form, before we publish the edited article. We will replace this Accepted Manuscript with the edited and formatted Advance Article as soon as it is available.

You can find more information about Accepted Manuscripts in the Information for Authors.

Please note that technical editing may introduce minor changes to the text and/or graphics, which may alter content. The journal's standard Terms & Conditions and the Ethical guidelines still apply. In no event shall the Royal Society of Chemistry be held responsible for any errors or omissions in this Accepted Manuscript or any consequences arising from the use of any information it contains.

ROYAL SOCIETY OF CHEMISTRY

rsc.li/chemcomm

ChemComm

COMMUNICATION

Fluorination-Controlled Supramolecular Polymerization and Piezoelectric Behavior

Received 00th January 20xx,
Accepted 00th January 20xx

DOI: 10.1039/x0xx00000x

Aritri Pal, [a] Swadesh Paul,[a†] Pradipta Kumar Das,[b†] Biman Jana,*[b] Anuja Datta*[c] and Suhrit Ghosh*[a]

This study explores fluorine-effect on the supramolecular polymerization and piezoresponse of naphthalene-diimide (NDI) derivatives. A single fluorine substitution in NDI-F induces higher crystallinity, thermal stability and cooperativity compared to its hydrogenated-analogue (NDI-H). Molecular dynamic simulation reveals that aligned C–F dipoles stabilize the supramolecular polymer via C-H---F interactions. Consequently, NDI-F exhibits a much superior piezoelectric coefficient (d_{33} ~ 24pm/V) than NDI-H.

Supramolecular polymers of π-systems[1-5] are produced primarily by hydrogen-bonding and π-stacking. Dipolar,[6] donor-acceptor charge-transfer[7-8] or metal-metal interaction,[9] halogen[10] or chalcogen bond [11] or other interactions have been employed only to a limited extent.[12-18] Fluorine is a unique element as its small atomic size and large nuclear charge generate the largest electronegativity of any element, which have found relevance in biology, synthetic chemistry or molecular materials.[19] We envisaged that fluorination could substantially control structure and functions of supramolecular polymers, which is yet to be explored. To test such possibilities, we have synthesized NDI-F (Fig 1a), in which a naphthalene-diimide (NDI) chromophore [20] is functionalized with an amide-linked branched hydrocarbon chain in one arm (for H-bonding), and a short chiral chain in the other arm (for macroscopic symmetry breaking). A single F atom is substituted in the beta-position to the imide-nitrogen to explore the fluorine-effect. NDI-H (Fig 1a) has otherwise same structure to NDI-F except the F atom. We envisaged, presence of the F atom might introduce extended C-H---F interaction [21] in the supramolecular polymer of NDI-F, which can impact its stability and structure due to the possibility of alignment of the C-F dipoles.[22]

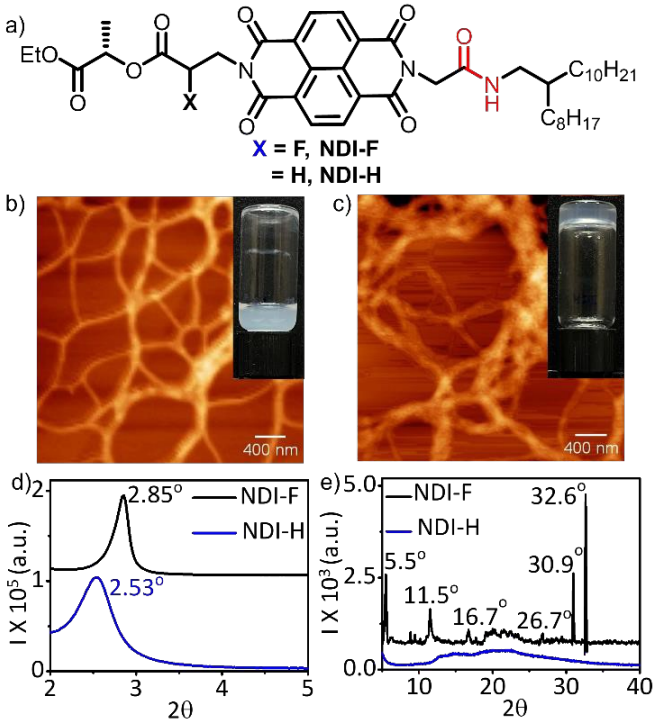

Fig. 1 (a) Structures of NDIF and NDI-H; AFM images of (b) NDI-F and (d) NDI-H in decane (c = 0.2mM), inset: sol/gel of (b) NDI-F and (d) NDI-H in decane; (c) Small angle and (e) wide angle powder XRD pattern of dried films of NDI-F and NDI-H.

Such dipole-alignment may lead to polarizable solid with piezoelectric properties.[23-25] NDI-F and NDI-H were synthesized (Scheme S1-4) in a few steps and isolated as off-white solid. Supramolecular polymerization of was examined in decane (c = 5.0 mM). When hot solution of NDI-F was cooled to rt, it did not produce gel (tested in the concentration window of 5-1.25 mM), but precipitated (inset-Fig 1b), unlike NDI-H showing gelation (inset-Fig 1c). Stress-amplitude sweep measurements (Fig S1)[26] with NDI-H gel revealed a linear viscoelastic region (LVR) with significantly larger storage modulus (G') than the loss modulus (G''), a typical characteristic of the gel phase. Despite this sharp

[a.] School of Applied and Interdisciplinary Sciences; Indian Association for the Cultivation of Science, Kolkata, India-700032.
[b.] School of Chemical Sciences; Indian Association for the Cultivation of Science, Kolkata, India-700032.
[c.] Department of Physics and Nanotechnology, SRM Institute of Science and Technology, Kattankulathur, India-603203; Current Address: Materials Systems Engineering, Max Planck Institute for Dynamics of Complex Technical Systems, Sandtorstraße 1, 39106 Magdeburg, Germany

† Contributed equally

contrast in gelation, AFM images (Fig 1b, c) indicated identical fibrillar network for both systems. Small-angle powder X-ray diffraction (PXRD) patterns of the dried films of NDI-F and NDI-H showed (Fig 1d-e) a single peak at 2θ = 2.53° (*d* = 35 Å) and 2.85° (*d* = 32 Å), for NDI-F and NDI-H, respectively. These *d*-spacings roughly correspond to the estimated end-to-end distance of the molecules along their long axis (Fig S2). However, in the wide-angle region, NDI-F showed multiple sharp peaks unlike NDI-H, indicating higher crystalline order for the NDI-F, which could be the reason for the macroscopic precipitation in this case.[27]

Supramolecular polymerization was further probed in dilute solution (*c* = 0.1 mM) by UV/Vis and CD spectroscopy (Fig 2). In THF, identical spectra exhibiting sharp absorption bands with vibronic peaks in the range of 300-400 nm, indicate monomeric state for both systems. In decane, bathochromic shift with significantly reduced peak intensity (Fig 2a) and reversal of the ratio of the intensity of the peaks at ~385 and ~365 nm (I_{385}/ I_{365}) suggests π-stacking [20] for both systems. A notable CD band in decane (Fig 2b) indicates transfer of molecular chirality to the supramolecular polymer. Variable temperature UV/Vis spectroscopy in decane (Fig S3) showed that with increasing temperature, the aggregated spectra gradually changed and eventually monomeric spectra were noticed at the elevated temperature. The melting curves (inset-Fig 2a) revealed $\alpha_{0.5}$(T) (temperature at which the mole fraction of aggregate = 0.5) to be 61 °C and 47 °C for NDI-F and NDI-H, respectively, indicating significantly higher thermal stability for NDI-F polymer. Thermodynamic parameters associated with supramolecular polymerization were estimated from the cooling curves obtained from UV/Vis spectroscopy (Fig S4). For both systems, non-sigmoidal curves were obtained (Fig S4), indicating cooperative supramolecular polymerization. Fitting of these curves (Fig S4) with the nucleation-elongation model,[28] reveal (Table S1) significantly higher T_e and smaller value of the dimensionless equilibrium constant K_a for NDI-F, indicating higher propensity of supramolecular polymerization and cooperativity in the supramolecular polymerization of NDI-F, which may be related to the dipole (C-F) alignment.[22]

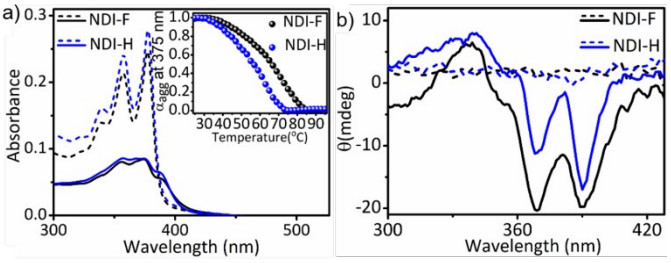

Fig. 2 (a) UV/vis spectra of NDI-F and NDI-H in THF (dashed line) or decane (solid line) (c = 0.1mM, l = 0.1 cm), inset: Variation of mole fraction of the aggregate (estimated from change in intensity at 375 nm for each case) as a function of temperature obtained from UV/vis spectra; (b) CD spectra of NDI-F (black), NDI-H (blue) in THF (dotted line) and decane (solid line) (c=0.2mM, l = 0.1 cm).

To probe the origin of these differences, we carried out molecular dynamics (MD) simulation (Fig 3, S5-6). Simulations of 40 initially dispersed molecules (NDI-H or NDI-F) revealed spontaneous stacking over the course of the trajectories, which was subsequently used as a basis for constructing higher-order configurations. To quantify the stability of pair-wise interactions, the potential of mean force (PMF) between two NDI molecules was computed in a dimeric setup (Fig 3a). A one-dimensional umbrella sampling approach was employed, using the distance between the centres of mass of adjacent NDI rings as the reaction coordinate.

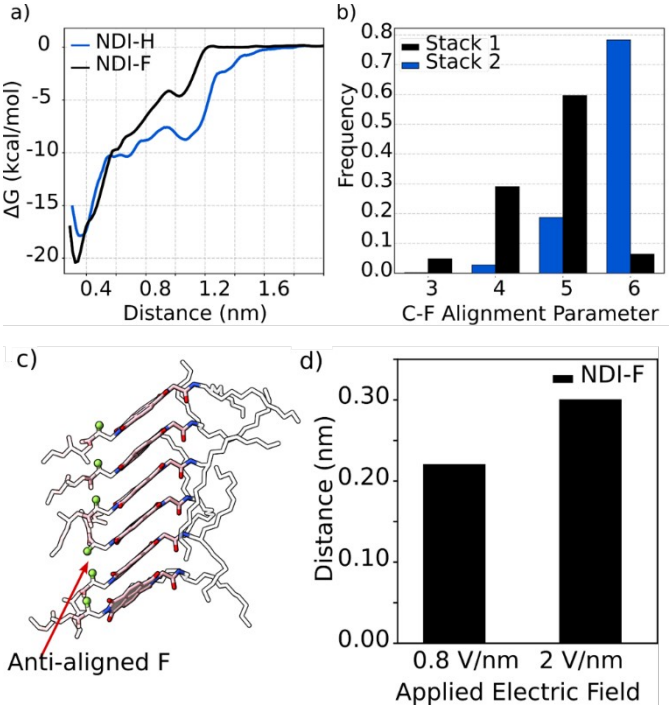

Fig. 3 (a) Potential of mean force (PMF) profile for dimer formation of NDI-H and NDI-F; (b) C-F alignment parameter calculated for the two intercalated octameric stacks. Higher values indicate a correlated orientation of C-F bond vector with respect to the stacking direction; (c) Octameric stack of NDI-F showing majority aligned C-F bonds; (d) Effect of applied electric fields (0.8 and 2 V/nm) on NDI aggregates. Distance differences were measured at the pentameric core along the field direction to minimize terminal fluctuations from the octameric stack. Relative to the zero-field condition, NDI-F shows progressive expansion with increasing field strength.

The resulting free energy profiles indicate that NDI-F exhibits a deeper minimum than NDI-H by approximately 2.5 kcal/mol (Fig 3a). Additionally, a secondary minimum at 1.1 nm corresponds to a vertically oriented configuration, where the molecules are stabilized by hydrogen bonding between amide groups (Fig S5). To further probe the stacking motif, representative configurations from these dispersed systems were propagated into tetrameric assemblies. In both cases, the dominant arrangement was found to be an offset stacking geometry. Building on the tetrameric stacking parameters, the assemblies were extended to octameric stacks (Fig 3c). However, a single stack alone did not exhibit sufficient stability over long timescales. To address this, a secondary stack was introduced in proximity to the primary one (Fig S6). The resulting double-stack configuration formed an intercalated architecture in which pendant groups interact not only within a given stack but also across neighbouring stacks, contributing to the overall stability. Structural inspection revealed the presence of specific C–F···H–C interactions between adjacent NDI-F molecules. To quantify this effect, a geometric descriptor was defined: the angle between the stacking vector (connecting adjacent NDI centres along the stacking direction) and the C–F bond vector of the

upper molecule among the two NDI molecules under consideration. Excluding terminal units, six such angles were evaluated over the trajectory. These angles were classified as aligned (< 90°) or anti-aligned (> 90°) relative to the stacking direction. A metric was constructed to quantify the degree of correlation, ranging from 3 (uncorrelated orientations) to 6 (fully correlated alignment or anti-alignment) (Fig 3b). Analysis of this observable revealed a significant population at values of 5 and 6 for NDI-F stacks, indicating a strong tendency toward correlated orientation of the C–F bonds along the stacking axis (Fig 3b, S7), likely contributing to the enhanced stabilization of NDI-F system by C-H---F interaction. This was supported by solvent and temperature dependent ^{19}F NMR spectroscopy (Fig. S8), revealing a net up-field shift $\Delta\delta(^{19}F) > 0.6$ ppm in decane compared to $CDCl_3$ or in decane as an elevated temperature. [29] Such oriented C-F generated a macro-dipole along the stack, desirable for piezoelectricity.[23-25] Distance changes induced by electric fields (0.8 or 2 V/nm) were quantified along the stacking direction of the bi-stacked octameric NDI-F aggregates which revealed significant expansion along the applied field direction by 0.22 nm at 0.8 V/nm and 0.30 nm at 2 V/nm for NDI-F, while it was much smaller for NDI-H, as also the net dipole moment of the pentameric stack (Fig. 3d, S9-10). Under the applied electric field, C-F bond ordering was further reinforced, resulting in near-complete alignment of the C–F bond vectors along the field direction in both stacks (Fig S16).

To probe the effect of such alignment of the C-F dipoles, intrinsic piezoelectric behaviour and nanoscale domain dynamics were investigated using piezoresponse force microscopy (PFM) and Kelvin probe force microscopy (KPFM). Switching spectroscopy PFM (SS-PFM) measurements were performed to probe local polarization switching in these NDI films. The SS-PFM butterfly loops and corresponding phase hysteresis curves (Fig 4a-b), recorded in the "off-state" after applying a sequence of DC biases between the conductive tip and ITO substrate, exhibit clear full phase switching (~180°) at a coercive voltage of ~3 V, confirming switchable polarization. The extracted effective piezoelectric coefficient ($d_{33\text{-eff}}$) value [30-31] (Table S1) for NDI-F (≈ 24 ± 3 pm/V) was found (Fig 4c) to be significantly larger compared to that of NDI-H (≈ 10 ± 3 pm/V) (Fig 4a), which is attributed to greater polarizability of NDI-F supramolecular polymer due to aligned C-F dipoles (Fig 3).

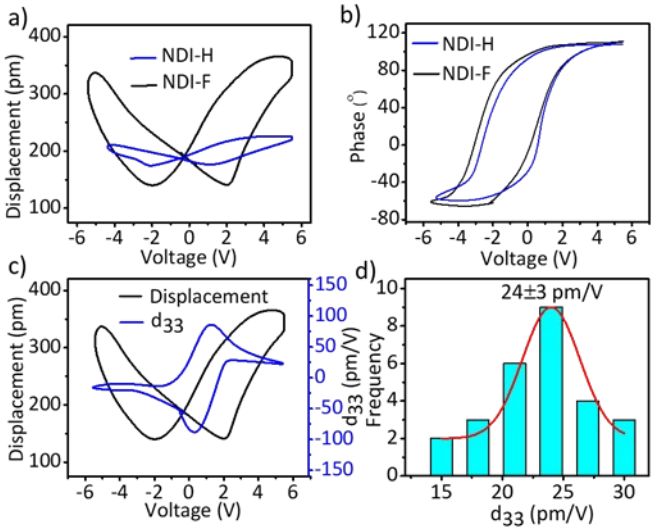

Fig. 4 (a) PFM butterfly hysteresis loops for the NDI-H and NDI-F molecules, showing field-dependent electromechanical response; (b) Phase hysteresis loop for NDI-H and NDI-F (c) PFM butterfly loop and corresponding d_{33} plot for the NDI-F supramolecular system, illustrating the field-dependent piezoelectric response. (d) Gaussian-fitted histogram of d_{33} with an average peak value ~ 24 pm/V.

The Gaussian-fitted histogram of d_{33}indicates the average piezoresponse of the sample (Fig 4d). Voltage-dependent SS-PFM studies further reveal that stable phase hysteresis loops are observed within a bias window of 2-6 V, defining a cut-off voltage of ~2 V and a breakdown voltage near ~7 V (Fig S11). T he widening of the phase hysteresis loop area with increasing bias likely reflects enhanced dipole alignment during repeated switching cycles, whereas minor ionic or charge-redistribution

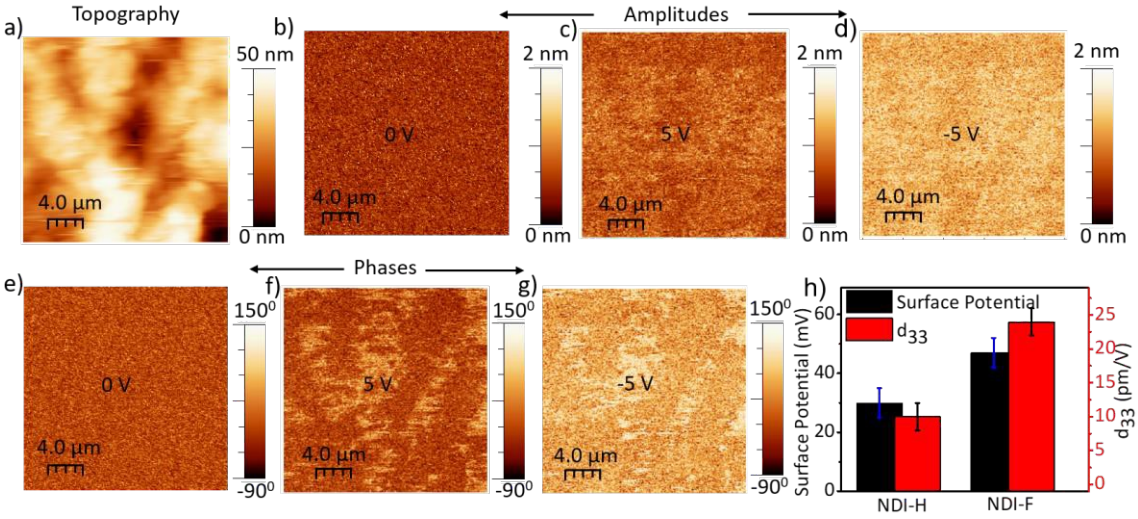

Fig. 5 (a) PFM topography image (a) amplitude image of the NDI-F supramolecular system at 0 V bias; (b-d) amplitude images of NDI-F under applied bias voltages of ±5 V, illustrating the variation in piezoresponse with field polarity; (e-g) PFM phase images of NDI-F under applied bias voltages of ±5 V, illustrating the variation in piezoresponse with field polarity , demonstrating the corresponding changes in polarization contrast and domain response; h) variation of the surface potential and d_{33} of the NDI-H and NDI-F supramolecular system.

contribution, if present, will be presumably similar in both NDI-F and NDI-H.[30-33] Moreover, NDI-F retains a significant piezoelectric response even after 100 continuous cycles, indicating reasonable stability for any supramolecular system (Fig. S11c, d). PFM imaging of NDI-F (Fig 5) and NDI-H (Fig S12), surface topography, amplitude and phase under ±5 V bias demonstrate the presence of well-defined polarizable domains at microscopic levels. The absence of direct correlation between topography (Fig 5a) and amplitude domain contrast confirms that the observed signal originates predominantly from intrinsic piezoelectric deformation rather than morphological artefacts (Fig 5b-d). The clear contrast reversal in phase images under opposite bias polarities indicates stable and reversible domain switching (Fig 5e-g), providing strong evidence of intrinsic piezoelectricity in NDI-F. PFM (d_{33}) and complementary KPFM analysis provides insight into the nanoscale electrostatic potential distribution, revealing a higher surface potential for NDI-F (~47 mV) compared to NDI-H (~30 mV) (Fig 5h, Table S1). This enhancement is associated with stronger dipole orientation and increased surface charge density, leading to improved internal electric fields and charge transport characteristics. The KPFM topography image, corresponding surface potential map, and line profile showing the variation of surface potential along the selected region for the NDI-H and NDI-F supramolecular systems are shown in Fig S13. Together, the PFM and KPFM results establish a direct link between polarization switching and surface potential, demonstrating that electromechanical and electrostatic responses are strongly coupled in this system. Dielectric measurements show that NDI-F possesses a stable electrodynamic behaviour with a decent dielectric constant $\varepsilon_r \approx 30$ compared to NDI-H with $\varepsilon_r \approx 21$, along with a relatively low dielectric loss (Fig S14a-b). The absence of any anomaly in the dielectric plot indicates that electronic conductivity dominates rather than ferroelectric transition. Overall, the combination of pronounced microscopic piezoelectric polarization and an elevated dielectric constant underscore the potential of NDI-F for advanced sensing and energy-harvesting applications.

Conclusions

In summary, we have demonstrated a successful strategy to control the supramolecular polymerization and tune the piezoelectric performance of naphthalene-diimide (NDI) derivatives via a single fluorine substitution. The introduction of the fluorine atom enhances the crystalline order, thermal stability, and cooperativity of the supramolecular polymerization process due to the alignment of C–F dipoles, which stabilize the assembly likely through C–H···F interactions. Consequently, the self-assembled NDI-F system exhibits a significantly improved piezo-response, which is comparable or higher than recently reported organic and supramolecular piezoelectric systems (Table S2). These findings highlight the potential of localized fluorination as an effective design principle for developing polar supramolecular polymers[34-43] for micro-power energy harvesting and bioelectronics.

Conflicts of interest

There are no conflicts to declare.

Data availability

The data supporting this article have been included as part of the Supplementary Information.

Notes and references

AP, SP and PKD thank IACS for a research fellowship. SG and AD thank ANRF (ARG/2025/000880/CS) for financial support

1 P. K. Hashima, J. Bergueiro, E. W. Meijer and T. Aida, *Prog. Polym. Sci.*, 2020, **105**, 101250.
2 Z. Chen, A. Lohr, C. R. Saha-Möller and F. Würthner, *Chem. Soc. Rev.*, 2009, **38**, 564.
3 S. S. Babu, V. K. Praveen and A. Ajayaghosh, *Chem. Rev.*, 2014, **114**, 1973.
4 Z. Fernández, L. Sánchez, S. S. Babu and G. Fernández, *Angew. Chem., Int. Ed.*, 2024, **63**, e202402259.
5 S. Cantekin, T. F. A. de Greef and A. R. A. Palmans, *Chem. Soc. Rev.*, 2012, **41**, 6125.
6 F. Würthner, *Acc. Chem. Res.*, 2016, **49**, 868.
7 M. Kumar, K. Venkata Rao and S. J. George, *Phys. Chem. Chem. Phys.*, 2014, **16**, 1300.
8 A. Das and S. Ghosh, *Angew. Chem., Int. Ed.*, 2014, **53**, 2038.
9 N. Bäumer, J. Matern and G. Fernández, *Chem. Sci.*, 2021, **12**, 12248.
10 S. Biswas and A. Das, *ChemNanoMat*, 2021, **7**, 748.
11 (a) A. Dhaka, I.-R. Jeon and M. Fourmigué, *Acc. Chem. Res.*, 2024, **57**, 362; (b) L. Vogel, P. Wonner and S. M. Huber, *Angew. Chem., Int. Ed.*, 2019, **58**, 1880.
12 J. J. B. van der Tol, G. Vantomme and E. W. Meijer, *J. Am. Chem. Soc.*, 2023, **145**, 17987.
13 S. Bujosa, A. Doncel-Giménez, N. Bäumer, G. Fernández, E. Ortí, A. Costa, C. Rotger, J. Aragó and B. Soberats, *Angew. Chem., Int. Ed.*, 2022, **61**, e202213345.
14 S. Sarkar, A. Sarkar, A. Som, S. S. Agasti and S. J. George, *J. Am. Chem. Soc.*, 2021, **143**, 11777.
15 K. Aratsu, R. Takeya, B. R. Pauw, M. J. Hollamby, Y. Kitamoto, N. Shimizu, H. Takagi, R. Haruki, S.-i. Adachi and S. Yagai, *Nat. Commun.*, 2020, **11**, 1623.
16 R. M. Veedu, Z. Fernandez, N. Baumer, A. Albers and G. Fernandez, *Chem. Sci.*, 2024, **15**, 10745.
17 M. A. Martínez, A. Doncel-Giménez, J. Cerdá, J. Calbo, R. Rodríguez, J. Aragó, J. Crassous, E. Ortí and L. Sánchez, *J. Am. Chem. Soc.*, 2021, **143**, 13281.
18 P. Khanra, A. K. Singh, L. Roy and A. Das, *J. Am. Chem. Soc.*, 2023, **145**, 5270.
19 D. W. Bruce, *Chem. Sci.*, 2025, **16**, 22213.
20 A. Das and S. Ghosh, *Chem. Commun.*, 2016, **52**, 6860.
21 R. Berger, G. Resnati, P. Metrangolo, E. Weber and J. Hulliger, *Chem. Soc. Rev.*, 2011, **40**, 3496.
22 C. Kulkarni, K. K. Bejagam, S. P. Senanayak, K. S. Narayan, S. Balasubramanian and S. J. George, *J. Am. Chem. Soc.*, 2015, **137**, 3924.
23 T. Vijayakanth, D. J. Liptrot, E. Gazit, R. Boomishankar and C. R. Bowen, *Adv. Funct. Mater.*, 2022, **32**, 2109492.
24 C. R. Bowen, H. A. Kim, P. M. Weaver and S. Dunn, *Energy Environ. Sci.*, 2014, **7**, 25.
25 S. Barman, A. Pal, A. Mukherjee, S. Paul, A. Datta and S. Ghosh, *Chem. Eur. J.*, 2024, **30**, e202303120.
26 R. G. Weiss, P. Terech, *Molecular Gels: Materials with Self-Assembled Fibrillar Networks*, *Springer*, New York, 2006.

27 P. Rajdev, S. Chakraborty, M. Schmutz, P. Mesini and S. Ghosh, *Langmuir*, 2017, **33**, 4789.
28 P. van der Schoot, in *Supramolecular Polymers*, ed. A. Ciferri, Taylor & Francis Group, London, 2005.
29 C. Dalvit, C. Invernizzi, and A. Vulpetti, *Chem. Eur. J.* 2014, **20**, 11058.
30 O. Kwon, D. Seol, H. Qiao, Y. Kim, *Adv. Sci.*, 2020, **7**, 1901391.
31 I. Urbanaviciute, X. Meng, M. Biler, Y. Wei, D. Cornelissen, S. Bhattacharjee, M. Linares, M. Kemerink, *Mater. Horiz.* 2019, **6**, 1688.
32 J.S. Sekhon, L. Aggarwal, G. Sheet, *Appl. Phys. Lett.* 2014, **104**, 162908.
33 S. Paul, A. Pal, S. Ghosh and A. Datta, *Chem. A Eur J.*2025, **31**, e202500540.
34 R. A. Whiter, V. Narayan and S. Kar-Narayan, *Adv. Energy Mater.*, 2014, **4**, 1400519.
35 D. Gupta, V. Gupta, D. Nath, C. Miglani, D. Mandal and A. Pal, *ACS Appl. Mater. Interfaces*, 2023, **15**, 25110.
36 A. Ramesh, T. N. Das, T. K. Maji and G. Ghosh, *Chem. Sci.*, 2024, **15**, 16355.
37 S. Paul, S. Barman, A. Pal, A. Mukherjee, S. Ghosh and A. Datta, *Chem. Mater.*, 2023, **35**, 6463.
38 Deepak, Z. Mallick, U. Sarkar, D. Mandal and R. K. Roy, *Chem. Mater.*, 2023, **35**, 3316.
39 U. Umesh, S. Bera and S. Bhattacharya, *Small*, 2024, **20**, 2308104.
40 Takeda, T.; Akutagawa, T. *Chem. Commun.*, 2022, **58**, 11898.
41 A. S. Tayi et. al. *Nature*, 2012, **488**, 485.
42 I. Urbanaviciute, X. Meng, T. D. Cornelissen, A. V. Gorbunov, S. Bhattacharjee, R. P. Sijbesma and M. Kemerink, *Adv. Electron. Mater.*, 2017, **3**, 1600530.
43 S. Paul and D. Chaudhuri, *Chem. Commun.*, 2025, **61**, 14366.

The data supporting this Communication have been included as part of the Supplementary Information.